

KMTNet Nearby Galaxy Survey II. Searching for Dwarf Galaxies in Deep and Wide-field Images of the NGC 1291 system

WOOWON BYUN,^{1,2} YUN-KYEONG SHEEN,¹ HONG SOO PARK,¹ LUIS C. HO,^{3,4} JOON HYEOP LEE,^{1,2}
SANG CHUL KIM,^{1,2} HYUNJIN JEONG,¹ BYEONG-GON PARK,^{1,2} KWANG-IL SEON,^{1,2} YOUNGDAE LEE,⁵
YONGSEOK LEE,^{1,6} SANG-MOK CHA,^{1,6} JONGWAN KO,^{1,2} AND MINJIN KIM⁷

¹*Korea Astronomy and Space Science Institute, Daejeon 34055, Korea*

²*University of Science and Technology, Korea, Daejeon 34113, Korea*

³*Kavli Institute for Astronomy and Astrophysics, Peking University, Beijing 100871, China*

⁴*Department of Astronomy, School of Physics, Peking University, Beijing 100871, China*

⁵*Department of Astronomy and Space Science, Chungnam National University, Daejeon 34134, Korea*

⁶*School of Space Research, Kyung Hee University, Yongin, Gyeonggi 17104, Korea*

⁷*Department of Astronomy and Atmospheric Sciences, Kyungpook National University, Daegu 41566, Korea*

(Received XXX; Revised YYY; Accepted January 2020)

Submitted to ApJ

ABSTRACT

We present newly discovered dwarf galaxy candidates in deep and wide-field images of NGC 1291 obtained with the Korea Microlensing Telescope Network. We identify 15 dwarf galaxy candidates by visual inspection. Using imaging simulations, we demonstrate that the completeness rate of our detection is greater than 70% for the central surface brightness value of $\mu_{0,R} \lesssim 26$ mag arcsec⁻² and for magnitudes $M_R \lesssim -10$ mag. The structural and photometric properties of the dwarf galaxy candidates appear to be broadly consistent with those of ordinary dwarf galaxies in nearby groups and clusters, with $\mu_{0,R} \sim 22.5$ to 26.5 mag arcsec⁻² and effective radii of 200 pc to 1 kpc. The dwarf galaxy candidates show a concentration towards NGC 1291 and tend to be redder the closer they are to the center, possibly indicating that they are associated with NGC 1291. The dwarf candidates presented in this paper appear to be bluer than those in denser environments, revealing that the quenching of star formation in dwarf galaxies is susceptible to the environment, while the morphology shaping is not.

Keywords: galaxies: dwarf – galaxies: individual (NGC 1291)

1. INTRODUCTION

The Λ CDM paradigm successfully predicts the large-scale structures of the Universe, but

it often fails to explain the properties on much smaller scales (see Bullock & Boylan-Kolchin 2017). Together with the too-big-to-fail (Boylan-Kolchin et al. 2011) and the planes of satellites problems (Pawlowski et al. 2012; Müller et al. 2017), one of the critical issues with this paradigm is the so-called ‘missing satellites

problem’ (Klypin et al. 1999; Moore et al. 1999) in which models predict that there are more satellite galaxies for a given host galaxy than are actually observed, based on the census of dwarf-scale satellite galaxies in the Local Group (LG).

There have been a lot of effort towards explaining the problems using cosmological simulations with higher resolution and much improved baryonic physics (see Section 3 in Bullock & Boylan-Kolchin 2017). Focusing on the possibility of incomplete observations, there have been several scenarios to explain the discrepancy between the predicted and observed number of satellite galaxies. One scenario suggests that tidal disruption of satellite galaxies can reduce the number of observable dwarf galaxies (e.g., Kravtsov et al. 2004; Garrison-Kimmel et al. 2017), but leaves behind distinct structures such as shells, streams, and tidal tails. It is also possible to mitigate the problem by applying physical mechanisms which suppress star formation in dwarf galaxies, such as supernovae-driven outflows (e.g., Font et al. 2011). Those processes leave remnants that would be expected to have a low surface brightness (LSB). In that respect, deep imaging surveys of LSB features are important as probes into the evolution of dwarf-scale satellite galaxies.

Since the 1980’s when LSB galaxies were first discovered (Sandage & Binggeli 1984), many studies have reported discoveries of those galaxies despite the surface brightness limit ($\mu_{0,V} \lesssim 26$ mag arcsec⁻²; e.g., Impey et al. 1988; Bothun et al. 1991; Dalcanton et al. 1997). Although intensive all-sky surveys, such as the Sloan Digital Sky Survey (SDSS; York et al. 2000), have made a tremendous contribution to this field, the detection of faint dwarf galaxies is still difficult because of their low surface brightness, which have a value less than 1% of the brightness of the night sky.

Table 1. Basic information of NGC 1291

Parameter	Value	Reference
R.A. (J2000)	03 ^h 17 ^m 18 ^s .6	1
Decl. (J2000)	−41°06′29″	1
Morphology	(R)SB0/a(s)	1
Distance	9.08 Mpc	2
M_{\star}	$\sim 8 \times 10^{10} M_{\odot}$	3
m_R	7.98 mag	4
r_e	$\sim 4\text{--}5$ kpc	4

References: (1) NASA Extragalactic Data base (NED); (2) McQuinn et al. (2017); (3) Li et al. (2011); (4) measured by Byun et al. (2018).

Recently, new observational strategies and data analysis techniques for deep imaging surveys have been progressively developed to explore the LSB nature in galaxy groups, clusters (e.g., Kim et al. 2011; Ferrarese et al. 2012; Cappacioli et al. 2015; van Dokkum et al. 2015; Mihos et al. 2015; Muñoz et al. 2015; Merritt et al. 2016; Venhola et al. 2017; Park et al. 2017; Kondapally et al. 2018; Smercina et al. 2018; Park et al. 2019), and fields (e.g., Javanmardi et al. 2016; Henkel et al. 2017; Leisman et al. 2017). Furthermore, automated detection methods for identifying faint dwarf galaxies have been contributed to much larger explorations (e.g., Merritt et al. 2014; Davies et al. 2016; Fliri & Trujillo 2016; van der Burg et al. 2016; Yagi et al. 2016; Bennet et al. 2017; Greco et al. 2018; Prole et al. 2018; Zaritsky et al. 2019; Carlsten et al. 2019). All of these efforts contribute to the detection of LSB galaxy populations and understand the evolution of dwarf galaxies in different environments.

In this paper, we present a list of dwarf galaxy candidates which are newly discovered in deep optical images of NGC 1291 taken by the Korea Microlensing Telescope Network (KMTNet; Kim et al. 2016b). NGC 1291 is located at

a distance of 9.08 Mpc (McQuinn et al. 2017) and there are two potential companion galaxies that have similar recessional velocities (see Section 4.2). The survey of the NGC 1291 system, which has been thought to be a low-density environment, can contribute to the study of environmental effects on the evolution of dwarf galaxies. The basic properties of NGC 1291 are presented in Table 1. The KMTNet imager contains four CCD chips with a field-of-view (FoV) of $\sim 1 \text{ deg}^2$ each, so the final mosaic images cover the whole area within the virial radius of NGC 1291¹. In this study, we assumed that all of the dwarf galaxy candidates are located at the same distance as NGC 1291.

This paper is organized as follows. Section 2 describes the outline of the observations and the data reduction process. Section 3 presents a list of dwarf galaxy candidates, the completeness of detections, and the properties of the discovered dwarf galaxy candidates. Section 4 discusses the implications of the results for the evolution of dwarf galaxy candidates. Section 5 summarizes the results.

2. DATA

We conducted deep optical imaging of NGC 1291 with KMTNet. Consisting of three 1.6-m identical telescopes, KMTNet is located at the Cerro Tololo Inter-American Observatory (CTIO), the South African Astronomical Observatory (SAAO), and Siding Spring Observatory (SSO). Each telescope contains a wide-field CCD camera with a $2^\circ \times 2^\circ$ FoV with average pixel scale of 0.4 arcsec. The data were taken at the KMTNet-CTIO observatory on November 12, 2015 with an average seeing of ~ 1.1 arcsec. A total of 85 *B*-band and 48 *R*-band

images were utilized which had total exposure times of ~ 2.8 and ~ 1.6 hrs, respectively. The images were taken by placing the target galaxy on each of the four chips with additional 7-points dithers. This strategy enabled us to obtain blank sky regions for dark-sky flat-fielding and also fill in the CCD gaps in the stacked images. The overall description of KMTNet Nearby Galaxy Survey (KNGS) project is also found in Byun et al. (2018).

The data reduction procedure used in this study is the same as that used in the previous study except for the addition of crosstalk correction (Kim et al. 2016a). We utilized crosstalk-corrected data this time to avoid confusing faint dwarf galaxies and artificial features. Brief description of the data reduction is as follows.

- *Overscan correction* was adopted to subtract bias level because of the apparent instability of the bias frames.
- *Dark sky flat* was generated by stacking all object frames with object-mask and then applied for flat-fielding.
- *A two-dimensional sky model* was subtracted from each object frame to remove gradients over the sky background.
- Accurate astrometric calibration was performed with SCAMP (Bertin 2006) following the instructions provided by the KMTNet project team².
- Stacked images were generated by SWarp (Bertin et al. 2002) using *median-combine* without photometric calibration.

Finally, we obtained deep mosaic images with a FoV of 12 deg^2 centered on NGC 1291 in the *B*- and *R*-bands. The photometric zero points for the mosaic images were determined using the

¹ To obtain the virial radius of NGC 1291, we adopted the conversion equation of $r_{1/2} \sim 0.015r_{200}$ (Kravtsov 2013). We assumed that the half-mass radius ($r_{1/2}$) can be replaced with the effective radius (r_e) because of a flat color profile in NGC 1291 (Byun et al. 2018).

² <http://kmtnet.kasi.re.kr>, “Astrometric calibration for KMTNet data”

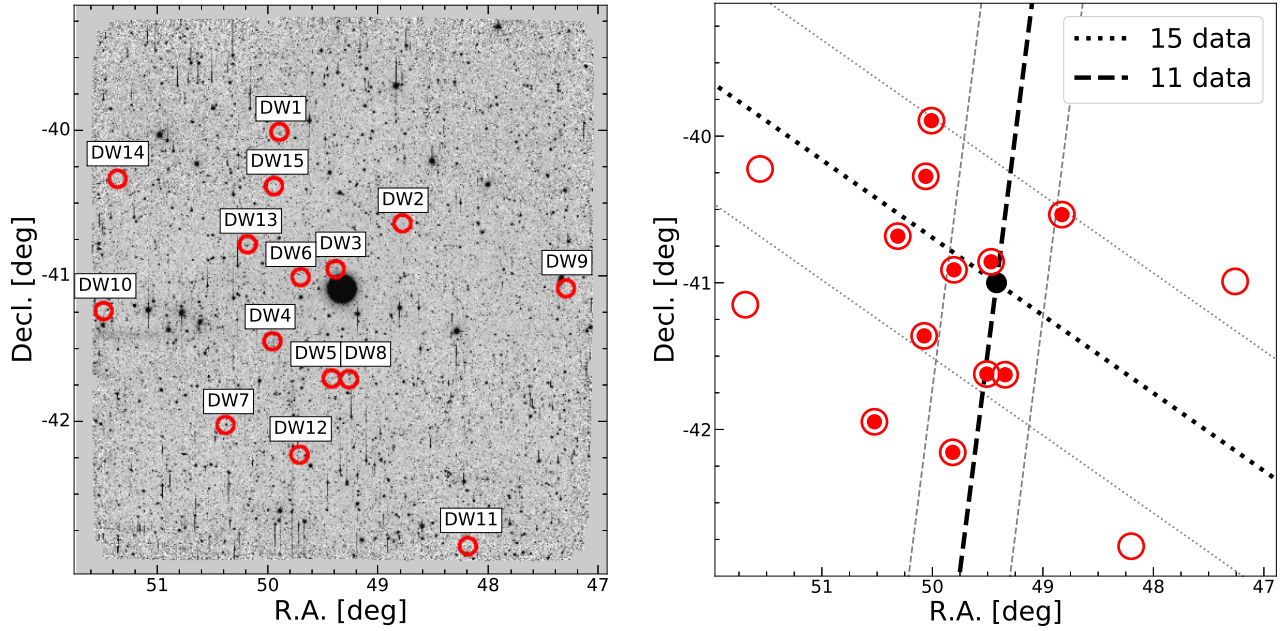


Figure 1. Left: The spatial distributions of 15 dwarf galaxy candidates (red circles) that we identified in the R -band mosaic image. NGC 1291 is located at the center. One side of the image is equivalent to ~ 600 kpc at the distance of NGC 1291. North is up and east is to the left. Right: The potential planes of satellite galaxies with the whole data (open circles; dotted line) and those relatively close to NGC 1291 (semi-filled circles; dashed line). The gray lines represent $\pm 1\sigma$.

AAVSO Photometric All-Sky Survey (APASS) DR9 catalog³. The optimized data reduction procedure allowed to investigate the surface brightness down to ~ 28 – 29 mag arcsec⁻² within 1σ limit.

3. RESULTS

3.1. Detection

Four of us (W. Byun, Y.-K. Sheen, H. S. Park, and M. Kim) performed visual inspection for searching faint dwarf galaxies, independently. The dwarf galaxy candidates had to (1) have similar appearances in both B - and R -band images; (2) exhibit a smooth gradation of surface brightness on their outskirts to distinguish them from massive background galaxies; and (3) not be located at the vicinity of bright

stars that may interfere with accurate identification. Each object discovered by each of us was then independently graded as “A/B/C”, where “A” is assigned to strong candidates with low surface brightness and extended light, “B” is assigned to ambiguous candidates with very low surface brightness, that can be easily confused with artifacts (e.g., crosstalk), “C” is assigned to less promising candidates with compact features. While a total of 35 objects were initially identified, we assessed that it might be biased by human subjectivity. Hence, we utilized the objects which are detected by at least two authors regardless of their grades. Then, we converted the grades “A/B/C” into the scores 25/15/5, and the objects with cumulative scores higher than 65 were designated as dwarf galaxy candidates. For the ambiguous candidates, several authors closely examined the images together for the final decision. This process resulted in the removal of proba-

³ <https://www.aavso.org/apass>, We derived R magnitude using the conversion equation $R = r - 0.1837 \times (g - r) - 0.0971$ provided by Lupton (2005)

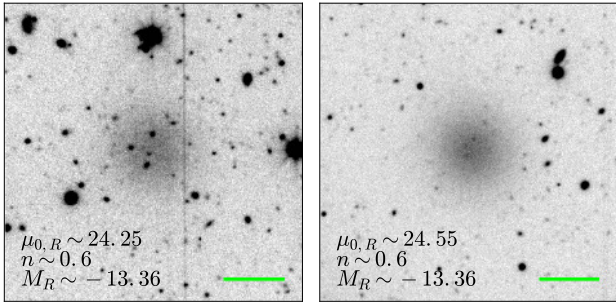


Figure 2. Comparison between the dwarf candidate N1291-DW4 (left) and a simulated dwarf galaxy (right). Both dwarfs share similar structural and photometric properties. The central surface brightnesses, Sérsic indices and absolute magnitudes are shown in the images. The horizontal bar at the bottom-right corresponds to 30 arcsec.

ble background objects and tidal features from the list. A total of 15 dwarf galaxy candidates were identified and their locations are shown in Figure 1. Four out of our candidates (N1291-DW6/DW7/DW8/DW14) had been previously detected (Morshidi-Esslinger et al. 1999; Paturel et al. 2003), but the rest are newly discovered in this study.

Interestingly, most of the dwarf candidates were located on the eastern side of NGC 1291 and were distributed from north to south. Indeed, such structures have been reported in other studies (e.g., Metz et al. 2007; Ibata et al. 2013; Merritt et al. 2014; Tully et al. 2015; Müller et al. 2017). If the satellites are isotropically distributed around the host galaxy, there must be no dependency for the specific direction. So we performed a total least square fit using the dwarf candidates to find potential plane structures. As seen in the right panel of Figure 1, we divided the sample into two subsamples taking into account the uncertainty of virial radius of NGC 1291: $D_{proj} \lesssim 300$ kpc (open circles) and $D_{proj} \lesssim 250$ kpc (semi-filled circles). When using the whole data set, the dwarf candidates seemed to be aligning with a large scatter from the northwest to the southwest (dotted lines). Meanwhile, when only 11

candidates were used, they seemed to be more tightly aligned along the north-south direction (dashed lines). Note that such analyses can be affected by a projection effect, so further spectroscopic observations may be needed to confirm the planarity of the satellite galaxies.

3.2. Imaging simulation

Imaging simulations were conducted to estimate the completeness of our visual inspection. Mock galaxies were generated on top of the mosaic image using `photutils` and `astropy.modeling` library in the PYTHON package. The mock galaxies were modeled by adopting the parameters of known dwarfs; (1) $-9.5 \leq M_R \leq -13.5$ mag, (2) $0.1 \leq r_e \leq 1$ kpc, (3) $0.5 \leq \text{Sérsic index } n \leq 1.0$, and (4) ellipticity $e \leq 0.6$. These mock galaxies were distributed randomly in the image and the line-of-sight distances were set to follow a Lorentzian distribution with a variance of ± 1 Mpc⁴ (cf. Smercina et al. 2018). The large wings in Lorentzian distribution can affect the completeness, but its effect appeared to be negligible because most of the simulated galaxies were located within a line-of-sight distance of ~ 300 – 400 kpc. Figure 2 compares a simulated galaxy with a dwarf galaxy candidate discovered in this study.

3.2.1. Completeness

Eight imaging simulations were performed. In each simulation, ~ 150 mock galaxies were generated. In order to estimate the completeness rate, the mock images were again subject to visual inspection. Note that we did not control the mock galaxies which are overlapped with bright objects, so the following results are presented as the lower limit. As shown in the left panel of Figure 3, the completeness rate reaches over $\sim 90\%$ for $M_R \lesssim -11.5$ mag in all galaxy

⁴ To reflect the actual distribution of dwarf galaxies in MW-like galaxies, we employ an additional constraint that $\sim 10\%$ of simulated galaxies have $\Delta d > \pm 0.4$ – 1 Mpc.

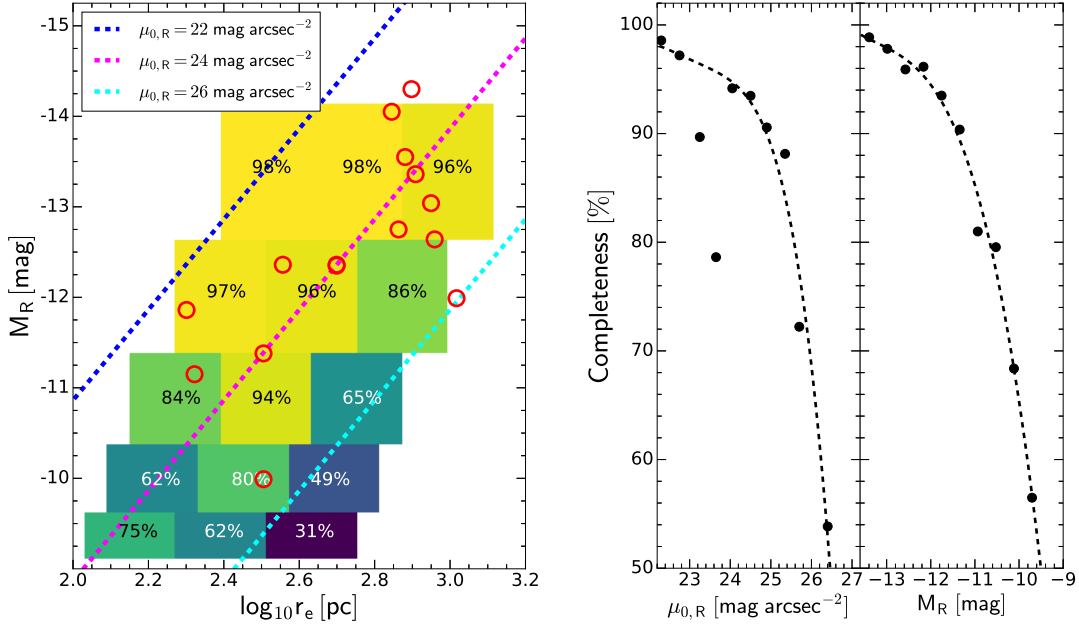


Figure 3. Left: Recovered fractions for simulated galaxies in absolute magnitude-effective radius space. The completeness rate of each bin is color-coded and noted. The red circles represent the dwarf galaxy candidates discovered in the NGC 1291 system. The dashed lines represent the central surface brightnesses of 22 (blue), 24 (magenta), and 26 (cyan) mag arcsec^{-2} when $n = 0.75$. Right: Completeness rates as a function of central surface brightness and absolute magnitude. The dashed lines are derived by quartic polynomial fit.

sizes and $\sim 70\%$ for $M_R \lesssim -10$ mag. Meanwhile, the completeness rate appears to be much sensitive to the galaxy size or central surface brightness for $M_R \gtrsim -11$ mag. This result is mainly due to confusion between small dwarf galaxies and massive background galaxies, and also partly induced by the 3σ surface brightness limit of ~ 26.5 mag arcsec^{-2} in the mosaic image (see Byun et al. 2018). The right panel of Figure 3 also shows the average completeness rates against central surface brightness and absolute magnitude. Although the points are sparsely distributed, the fitted curves support that the completeness rate reaches over $\sim 70\%$ for $M_R \lesssim -10$ mag and $\mu_{0,R} \lesssim 26$ mag arcsec^{-2} .

3.3. Structural and photometric properties

This section presents the properties of the dwarf galaxy candidates mainly using R -band images (Table 2).

The images were prepared by subtracting the sky background from each cutout image using a two-dimensional polynomial model. Note that the sky subtraction was performed before the mosaic images were generated, but there local sky fluctuations may have introduced residuals. The surface brightness profiles of the dwarf galaxy candidates were estimated in B - and R -band images using the ELLIPSE task in IRAF. All parameters were first fit freely. Then the central position, ellipticity, and position angle values at the effective radius of each dwarf candidate were conservatively calculated based on the initial results. Finally, the isophotal fit was performed again using the three values above as fixed parameters over the whole radius.

Figure 4 shows both the original and model-subtracted cutout images. Most of the removed objects left no residuals, but some (N1291-DW7/DW14) left irregular features due to their clumpy structures. Note that they seem like

Table 2. Catalog of the Dwarf Galaxy Candidates in the NGC 1291 system

ID	R.A.(J2000)	Decl.(J2000)	m_R^a	$B - R^b$	$\mu_{0,R}^c$	n^c	r_e^c	M_R^d	$\log M_\star^e$
	(hh:mm:ss)	(dd:mm:ss)	(mag)	(mag)	(mag arcsec $^{-2}$)		($''$)	(mag)	(M_\odot)
N1291-DW1	3:19:25.9	-40:03:47	17.46±0.13	1.31	24.18±0.19	0.65±0.03	11.30±0.23	-12.34	6.97
N1291-DW2	3:15:09.7	-40:40:05	17.05±0.13	1.17	24.61±0.19	0.65±0.03	16.62±0.38	-12.75	7.03
N1291-DW3	3:17:29.4	-40:58:22	16.25±0.05	1.36	23.81±0.07	0.71±0.01	17.30±0.17	-13.55	7.45
N1291-DW4	3:19:43.1	-41:26:54	16.44±0.08	1.28	24.25±0.13	0.60±0.02	18.47±0.26	-13.36	7.42
N1291-DW5	3:17:38.1	-41:41:45	16.76±0.10	1.16	24.57±0.14	0.77±0.02	20.32±0.42	-13.04	7.15
N1291-DW6 ^f	3:18:43.0	-41:01:27	17.44±0.18	1.14	23.09±0.24	0.88±0.04	8.24±0.17	-12.36	6.87
N1291-DW7 ^f	3:21:24.4	-41:59:44	15.50±0.04	1.13	23.34±0.06	0.58±0.01	17.86±0.14	-14.30	7.48
N1291-DW8 ^f	3:17:01.4	-41:42:01	15.75±0.10	1.23	22.95±0.13	0.82±0.02	15.88±0.24	-14.05	7.59
N1291-DW9	3:09:25.1	-41:04:57	18.42±0.18	1.20	23.90±0.23	0.84±0.04	7.37±0.14	-11.38	6.47
N1291-DW10	3:25:38.4	-41:13:51	17.16±0.23	1.11	25.08±0.32	0.72±0.05	20.60±0.82	-12.64	6.99
N1291-DW11	3:12:44.2	-42:47:54	17.51±0.32	0.81	23.99±0.44	0.80±0.07	11.63±0.54	-12.36	6.59
N1291-DW12	3:18:47.0	-42:11:58	19.81±0.36	1.12	25.19±0.54	0.75±0.09	7.22±0.26	-9.99	5.98
N1291-DW13	3:20:33.8	-40:48:18	17.81±0.34	1.22	26.39±0.55	0.48±0.08	23.60±1.89	-11.99	6.62
N1291-DW14 ^f	3:25:02.8	-40:21:32	17.94±0.48	1.02	22.66±0.63	0.80±0.11	4.56±0.18	-11.86	6.45
N1291-DW15	3:19:37.7	-40:25:17	18.65±0.32	1.07	22.83±0.38	1.07±0.22	4.82±0.22	-11.15	6.20

NOTE—Magnitudes and surface brightnesses are uncorrected for Galactic extinction.

^a Apparent magnitude calculated by Eq. 2.

^b Color measured within 2 effective radius derived from R -band image.

^c Central surface brightness ($\mu_{0,R}$), Sérsic index (n) and effective radius (r_e) in R -band image derived from the 1-D profile fit.

^d Absolute magnitude calculated by assuming that the dwarfs are at the same distance as NGC 1291 ($d = 9.08$ Mpc).

^e Stellar mass estimated with an equation of $\log(M_\star/L) = 0.872 \times (B - R) - 0.866$ adopted from [Into & Portinari \(2013\)](#).

^f Cross-ID: [MDS99] F301-056, [MDS99] F301-044, [MDS99] F301-064, LEDA 587327, respectively.

background spiral galaxies, but their central surface brightnesses are somewhat fainter than that of the typical spiral galaxies ($\mu_{0,B} \sim 21.65$ mag arcsec $^{-2}$; see [Bosma & Freeman 1993](#) and references therein), implying that they are likely to be dwarf galaxies. Several dwarf spiral galaxies have been found in the nearby Universe although they are rare (cf. [Schombert et al. 1995](#); [Lisker et al. 2006](#)). However, without any confirmation of their distances, it is hard to determine the real nature of them.

The azimuthally averaged surface brightness and color profiles are also presented in Figure 4. Note that the parameters presented in this section are not corrected by foreground Galactic extinction because the expected reddening effect towards NGC 1291 is negligible at $E(B - V) \sim 0.01$.

The central surface brightnesses of the candidates are distributed between $22.5 \lesssim \mu_{0,R} \lesssim 26.5$ mag arcsec $^{-2}$ and their average central surface brightness is $\mu_{0,R} \sim 24.05$ mag arcsec $^{-2}$. The surface brightness profiles were fitted with a single Sérsic function which is commonly expressed as

$$I(r) = I_e \exp \left\{ -b_n \left[\left(\frac{r}{r_e} \right)^{1/n} - 1 \right] \right\}, \quad (1)$$

where r_e is the effective radius, I_e is the intensity at the effective radius, n is the Sérsic index, and $b_n = 1.9992n - 0.3271$, a constant adopted from [Capaccioli \(1989\)](#) (see also [Ciotti & Bertin 1999](#)). Data points within the innermost 2 arcsec and which are fainter than 28 mag arcsec $^{-2}$ were not used for the fit. As a result, all dwarf galaxy candidates were well described

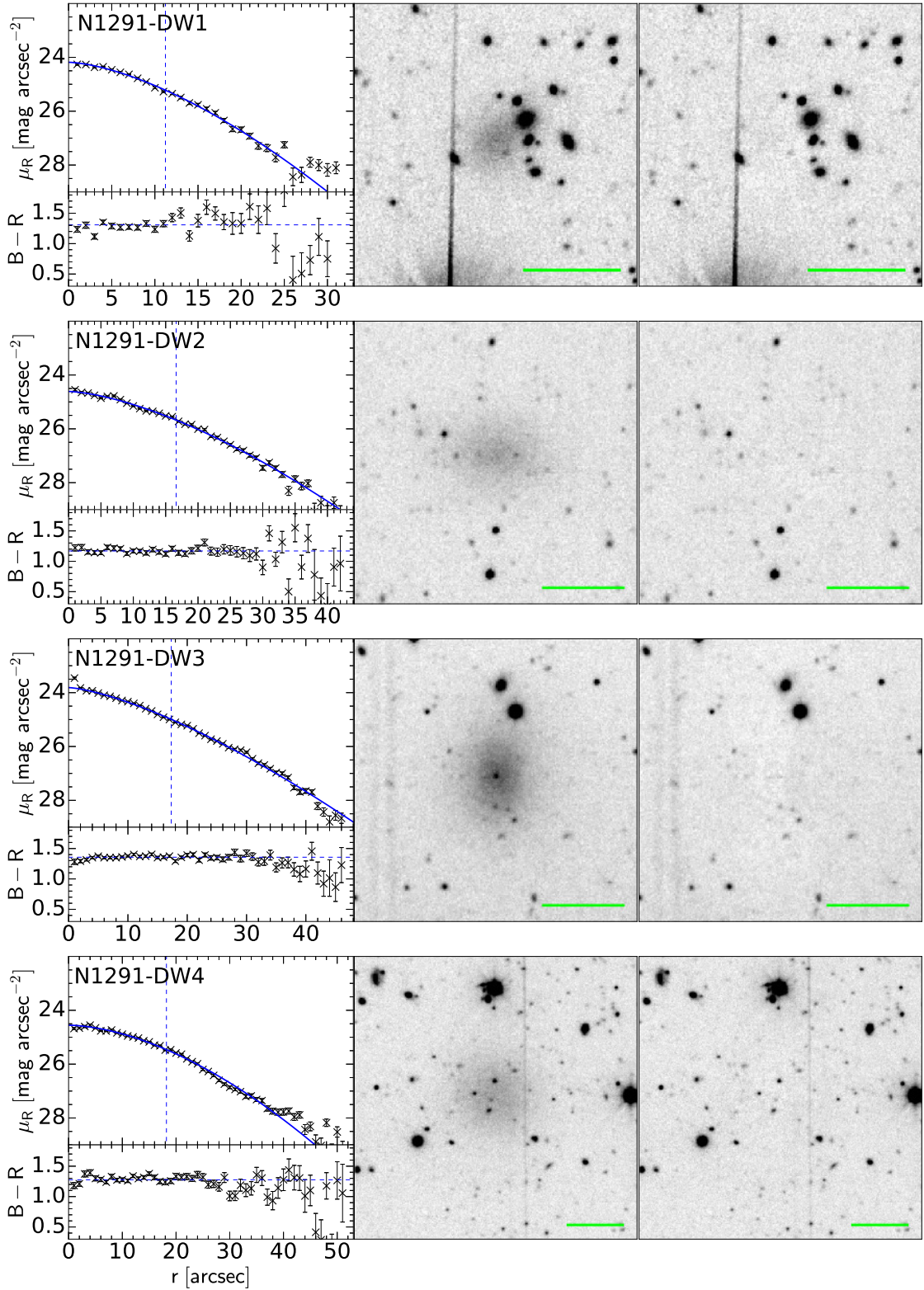


Figure 4. The surface brightness and color profiles (left), R -band cutout images (middle), and residuals (right) of dwarf galaxy candidates as a result of isophotal fit. The blue solid lines in the left panels represent a single Sérsic function. The blue dashed lines show the effective radii (vertical) and weighted mean colors (horizontal), respectively. The scale bar in the cutout images corresponds to 30 arcsec.

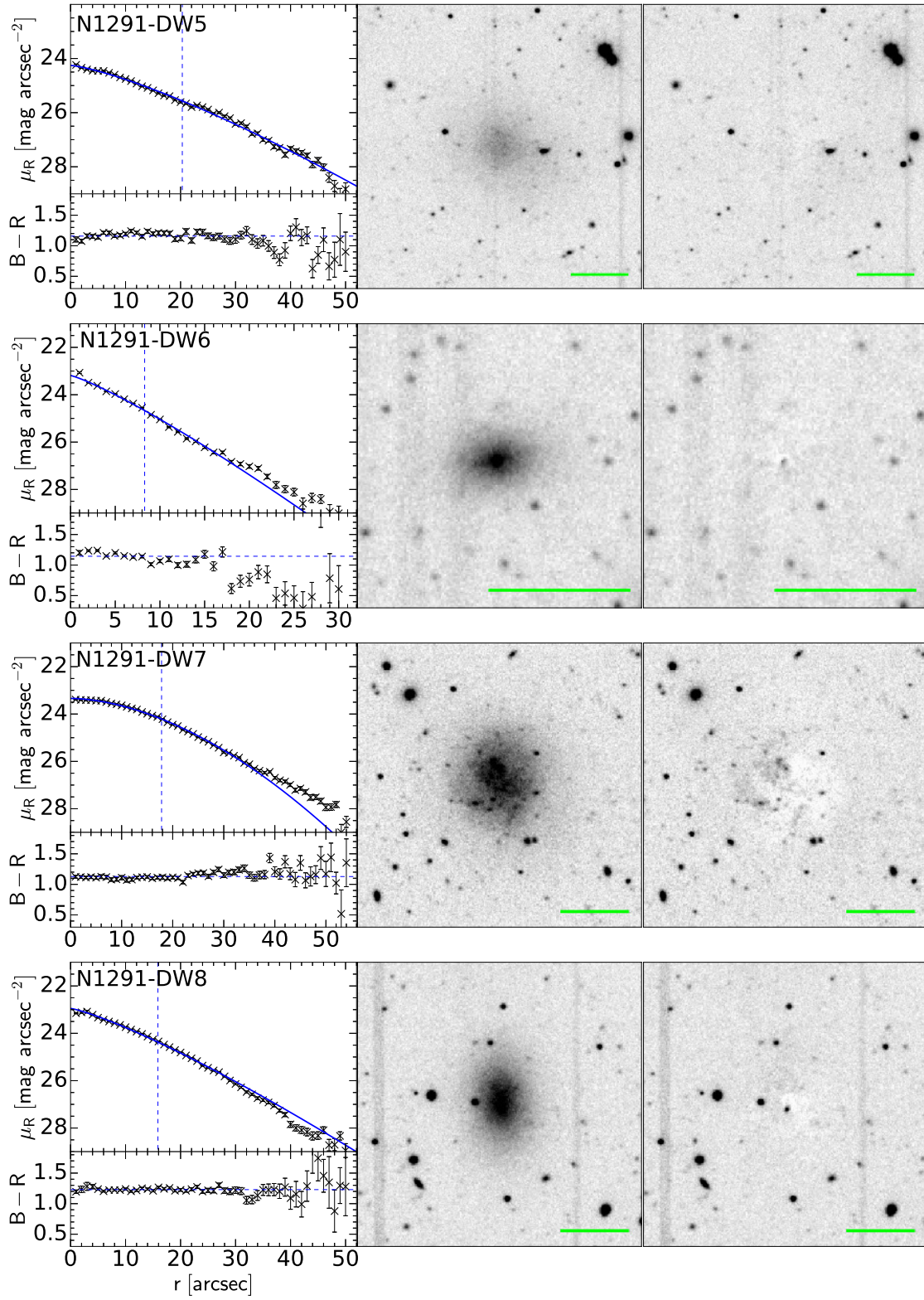


Figure 4. (Continued)

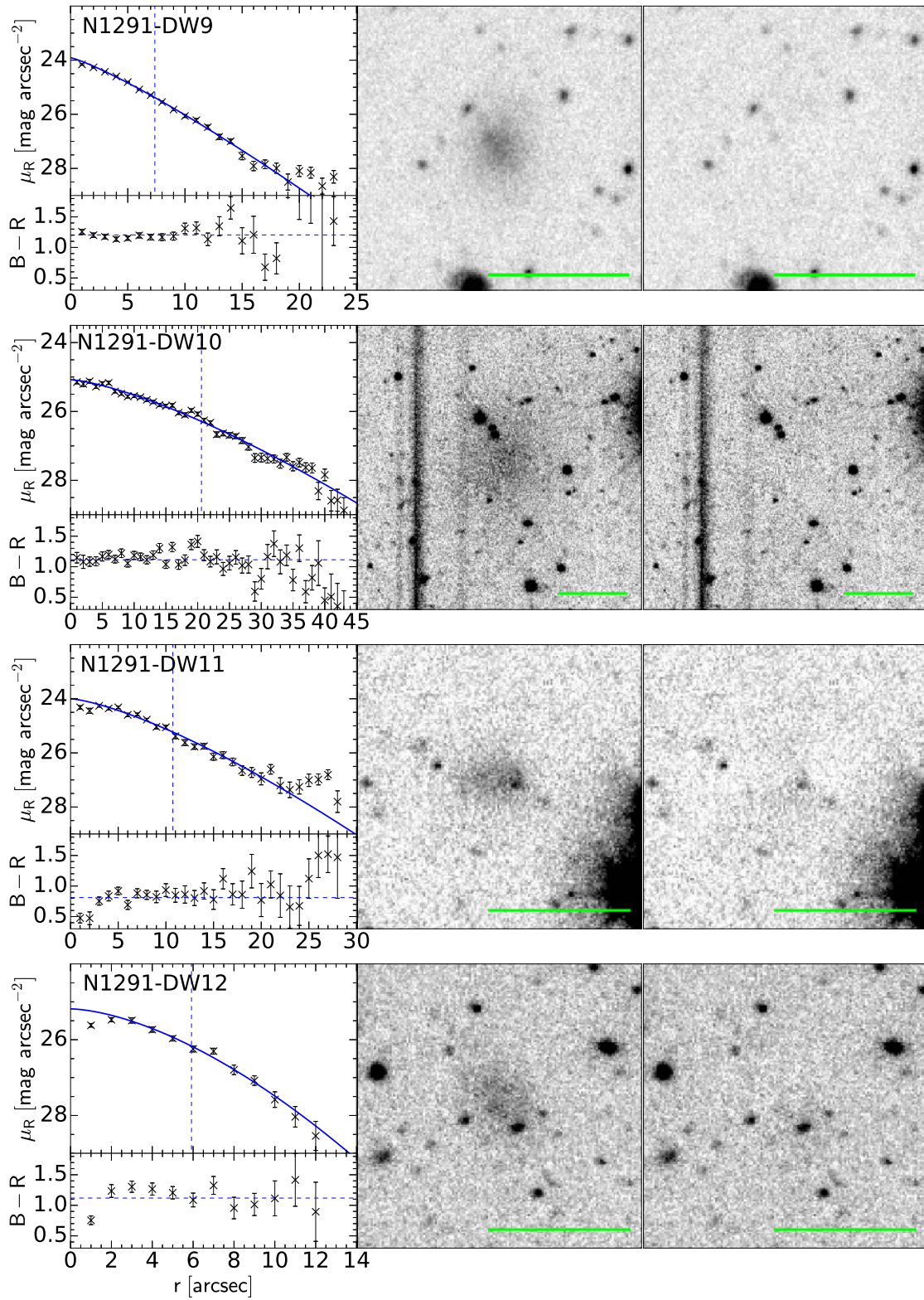


Figure 4. (Continued)

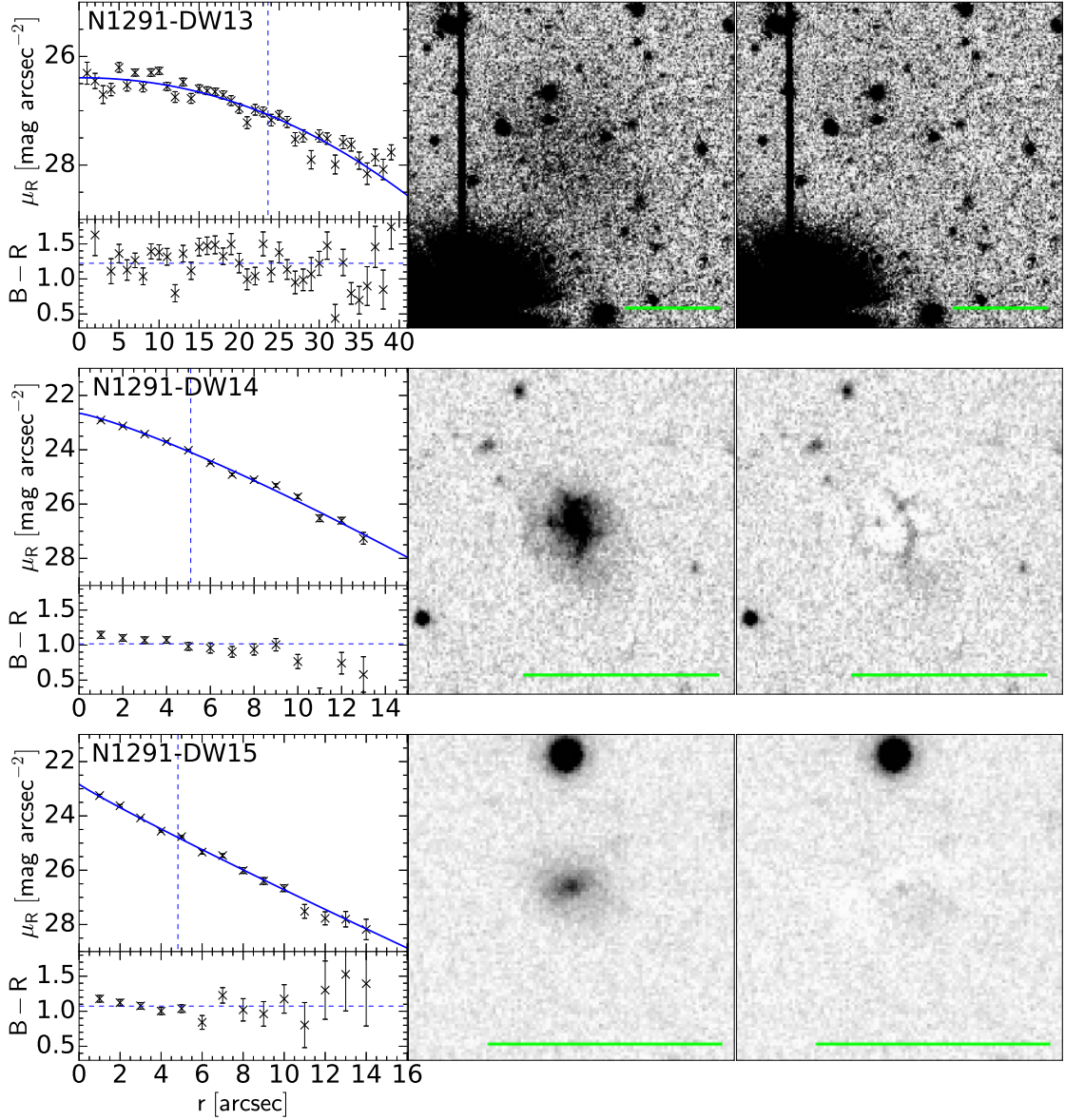


Figure 4. (Continued)

with a single Sérsic fit (blue solid lines in Figure 5). The effective radii were estimated to be $4.5 \lesssim r_e \lesssim 23.5$ arcsec (vertical lines in Figure 4). At a distance of 9.08 Mpc, it corresponds to $r_e \sim 200$ pc to 1 kpc. Sérsic indices were $0.5 \lesssim n \lesssim 1.0$ with an average value of 0.74. The total magnitudes of the dwarf galaxy candidates were estimated to be $15.5 \lesssim m_R \lesssim 20.0$ mag using the following equation of

$$L_{tot} = 2\pi I_0 r_s^2 n \Gamma(2n), \quad (2)$$

where I_0 is the intensity at the center, r_s is the scale length that satisfies the equation of $r_e \approx r_s (1.9992n - 0.3271)^n$, and Γ is the gamma function. Note that considering the image depth difference and large errors, there was no significant difference with the literature results of the four previously detected galaxies in terms of the central surface brightnesses and the apparent magnitudes.

The weighted average colors are shown as horizontal dashed lines in Figure 4. The color range

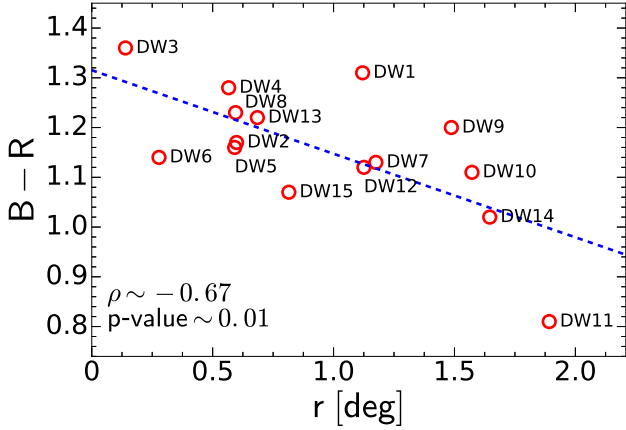


Figure 5. $B - R$ color distribution of the dwarf candidates as a function of their projected distance from the center of NGC 1291. The dashed line shows a linear fit with 15 dwarf galaxy candidates. The correlation coefficient and p-value are noted at the bottom of the panel.

is $0.8 \lesssim B - R \lesssim 1.5$ mag and the average value is $\langle B - R \rangle \sim 1.16$ mag. Taking into account large errors in the outer regions, most of the candidates exhibited weak or no gradients in their color profiles.

Furthermore, their stellar masses were calculated using the mass-to-light ratio of $\log(M_*/L) = 0.872 \times (B - R) - 0.866$ from exponential star formation history with Kroupa initial mass function developed by [Into & Portinari \(2013\)](#). The average stellar mass is $\sim 1.35 \times 10^7 M_\odot$. The stellar masses were also estimated using other mass-to-light ratios found in [Bell & de Jong \(2001\)](#) to quantify the uncertainty of the stellar masses. The deviation for estimating stellar mass was revealed up to $\sim 20\%$. Note that detailed stellar evolution uncertainty was not considered, so the true deviation may be much larger (cf. [Conroy 2013](#)).

Figure 5 shows the $B - R$ color distribution of the dwarf galaxy candidates as a function of their projected distance from the center of NGC 1291. Though the candidates are significantly scattered, there seems to be a negative linear correlation, which has also been reported in

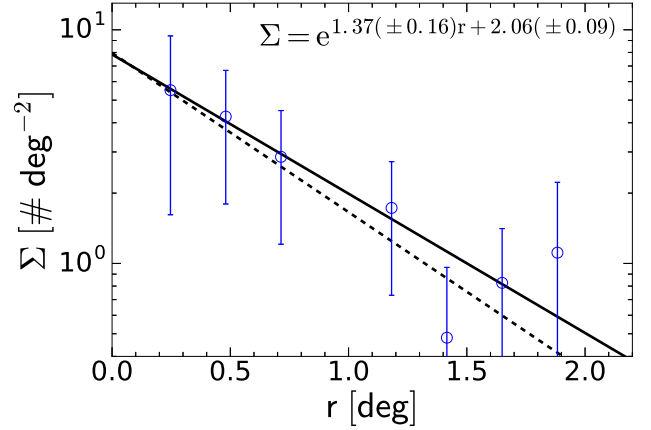


Figure 6. The radial number density profiles of the dwarf galaxy candidates which show the results from two different binning methods: the equal linear distance binning (solid line) and the equal area binning (dashed line). The data points and the equation were derived from the former method.

much massive environments (e.g., [Venhola et al. 2019](#)). Note that the color of dwarf galaxies can be affected by their masses and magnitudes (e.g., [Binggeli et al. 1985](#); [Conselice et al. 2002](#); [Adami et al. 2006](#); [Lieder et al. 2012](#); [Yagi et al. 2016](#)). We found that the color of the dwarf candidates are weakly correlated with the absolute magnitudes, but there is no statistically significant correlation between the total magnitudes and the projected distances. Indeed, [Phillips et al. \(2015\)](#) have reported that the quenching process of the satellite galaxies around isolated MW-like host galaxies can be effective at lower stellar masses ($< 10^8 M_\odot$). Therefore, a negative color gradient for the projected distance can be interpreted as a result of the quenching process of the satellite galaxies in the halo of NGC 1291 which also implies that the dwarf candidates may be accompanying NGC 1291.

Interestingly, N1291-DW3 and DW6 show weak excess of light in their innermost regions as nucleated cores. Given that they are the nearest candidates to NGC 1291, the nucleated core was likely a product of the tidal perturbation between the host and the satellite galax-

ies (cf. Binggeli & Cameron 1991; Oh & Lin 2000). However, the exact mechanism behind nucleation in dwarf galaxies is still a subject of debate (cf. Grant et al. 2005 and references therein). Moreover, Park et al. (2019) mentioned that the environment in different dynamic states can affect the correlation between the nucleated fraction and other physical properties of dwarf galaxies. More surveys of dwarf galaxies must be conducted, especially of those in environments similar to the one found in the NGC 1291 system.

3.4. Number density profile

Figure 6 presents two different radial number density profiles for the dwarf galaxy candidates according to their projected distance from the center of NGC 1291. The small sample size made the fit sensitive to the binning size, so two binning sizes were used: (1) equal linear distance in each annulus and (2) equal area in each annulus. Each can be well described by an exponential function up to the virial radius of NGC 1291. The two methods yielded the number densities of $\Sigma = e^{1.37(\pm 0.16)r+2.06(\pm 0.09)}$ and $\Sigma = e^{1.57(\pm 0.56)r+2.07(\pm 0.38)}$, respectively. These results are relatively similar and within the error budget. It may be inappropriate to extract physically meaningful results from this fit because of the limited sample size on which it was based, but it is worth noting that the number density profiles showed centrally concentrated distributions, implying that the dwarf candidates are associated with NGC 1291.

4. DISCUSSION

4.1. Comparisons with dwarfs in other host systems

NGC 1291 has been thought to reside in a relatively isolated environment. For instance, NGC 1291 accompanies a single bright galaxy ($M_R < -17$ mag) and 15 dwarf galaxy candidates within the projected distance of $D_{proj} < 300$ kpc. If the properties of dwarf galaxies are

easily affected by the environment, the comparison between the dwarf candidates discovered in this study and those in other host systems with different populations can provide useful insight into the evolution of dwarf galaxies. The following samples were chosen because they provided available data on structural and photometric properties of their satellites, regardless of their distance confirmations using resolved individual stars.

Figure 7 presents the effective radii, central surface brightnesses, and Sérsic indices of the dwarf candidates as a function of absolute magnitude. For the sake of simplicity, we assumed that the dwarf candidates are located at the distance of NGC 1291 (~ 9.08 Mpc). The properties of known dwarfs in other host systems as well as the Fornax cluster are also presented. The structural and photometric properties of the dwarf candidates in the NGC 1291 system were revealed to be similar to those in other environments. Their significant distribution indicates that the shapes of dwarf galaxies are independent of their environments. This finding also supports the assumption that the dwarfs are located at approximately the same distances as NGC 1291. In fact, it cannot be a robust evidence as a shift in their distances would not entirely separate them from a distribution with the bulk of dwarf galaxies. However, most of the dwarf candidates are unlikely to be located in the foreground or background because no other host systems is found in the images that may be associated with dwarf candidates.

We also compared the colors of the dwarf candidates with those provided from the literatures. Interestingly, the average color of the dwarf galaxy candidates, $(\langle B - V \rangle_0 \sim 0.63 \pm 0.10)^5$, is slightly smaller than that of the dwarfs in the

⁵ We used the interpolated conversion factors of $V - R$, matching to the $B - R$ color of each candidate adopted from Fukugita et al. (1995)

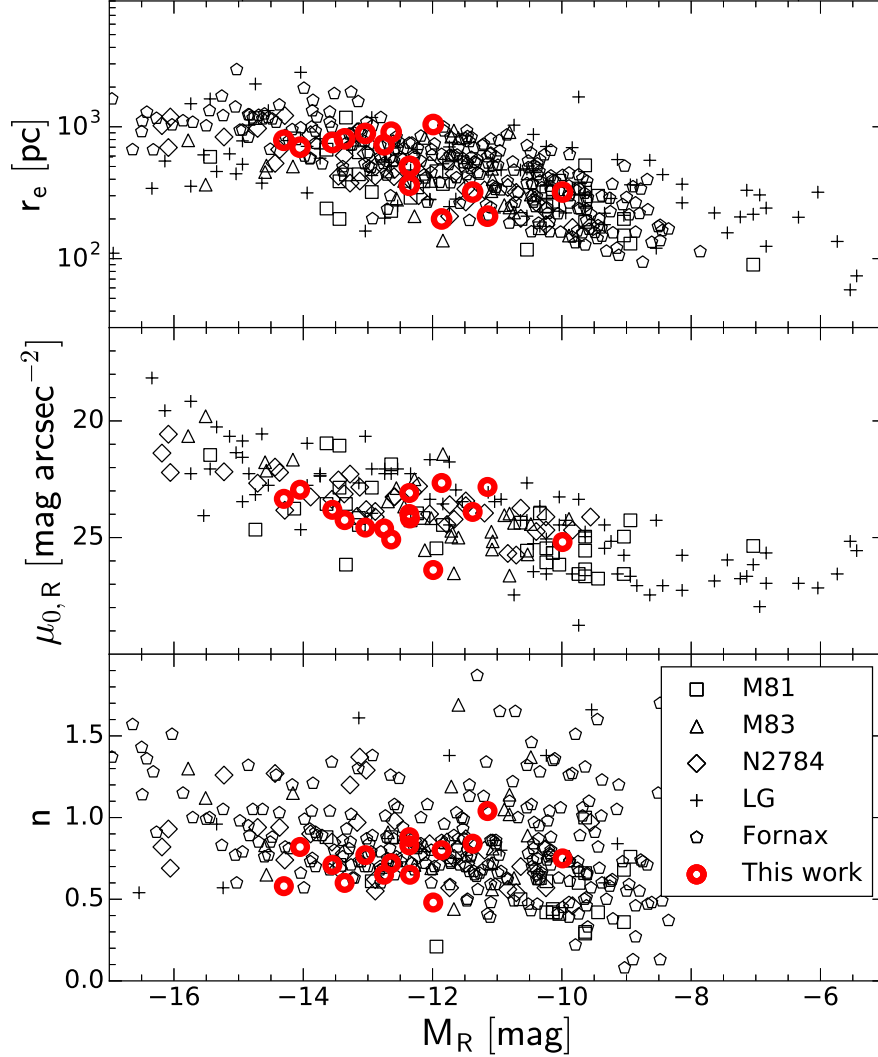


Figure 7. The effective radii, central surface brightnesses, and Sérsic indices of dwarf galaxies as a function of absolute magnitude. Red circles denote the NGC 1291 candidates located at a distance of 9.08 Mpc. The squares, triangles, diamonds, crosses, and pentagons represent the dwarf galaxies in the M81 group (Chiboucas et al. 2009), the M83 group (Müller et al. 2015), the NGC 2784 group (Park et al. 2017), the LG (Jerjen et al. 2000; McConnachie 2012), and the Fornax cluster (Muñoz et al. 2015), respectively.

M83 group (0.82 ± 0.24 ; Müller et al. 2015), the M101 group (0.71 ± 0.04 ; Merritt et al. 2014), the M106 group (0.70 ± 0.19 ; Kim et al. 2011), and the NGC 2784 group (0.67 ± 0.17 ; Park et al. 2017). Note that the corrections for Galactic extinction were performed for all five samples and the $B - V$ colors in other studies were converted from g and r -band using the equation of Lupton (2005) if necessary. Indeed, this result may be inconclusive because of marginal uncer-

tainties in color measurement, and systematic differences among the studies in the observational conditions. Nevertheless, we suggest that the comparison of color distributions under the strict conditions will be helpful in exploring the evolution of dwarf satellite galaxies in different host systems.

The color of dwarf satellite galaxies can be affected by their own masses and their projected distances from their host galaxies, which

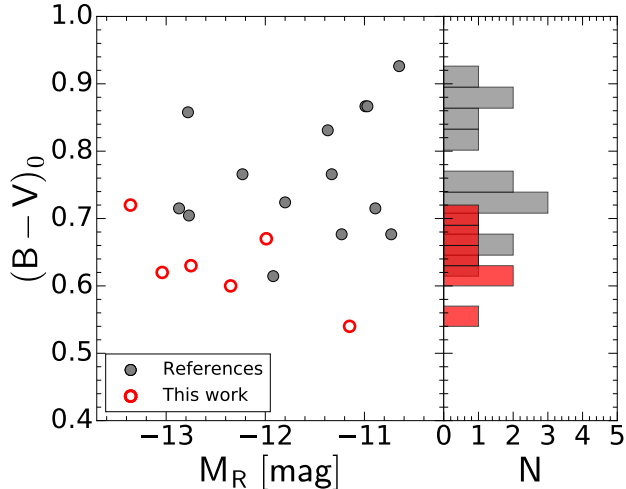


Figure 8. The color distributions of dwarf candidates in the NGC 1291 system (red) and those of the M83, M101, M106, NGC 2784 groups (gray). The samples had to meet the criteria of $D_{proj} \leq 130$ kpc and $-13.5 \leq M_R \leq -10.5$ mag.

as shown in Figure 5. Therefore, we utilized subsamples with the absolute magnitude range of $-13.5 \leq M_R \leq -10.5$ mag to avoid the mass effect as well as the incomplete detection issue. Secondly, we used the projected distance cut with $D_{proj} \leq 130$ kpc, adopted from the FoV limit of M106 survey (Kim et al. 2011). Note that the projected distance limit is broadly consistent with a half of the virial radius of each system, so dwarf galaxies within it are expected to have sufficiently experienced the environmental effect.

Figure 8 shows the color distributions of dwarf candidates in the NGC 1291 system and other dwarf galaxies. Approximately 15 dwarfs in the M83, M101, M106, NGC 2784 groups were selected as counterparts and their average color is $\langle B - V \rangle_0 \sim 0.76 \pm 0.09$. Six of the dwarf candidates in the NGC 1291 system were selected with an average color of $\langle B - V \rangle_0 \sim 0.63 \pm 0.06$. The Kolmogorov-Smirnov test also indicated that the color distributions of the two samples are unlikely to have been drawn from the same population (p-value $\simeq 0.01$). The dwarf candidates in the NGC 1291 system seem to have

magnitude-dependent color distributions, while dwarf galaxies in other host systems tend to be redder regardless of their absolute magnitudes. This difference tends to be more obvious in less luminous dwarf galaxies which are thought to be susceptible to environmental effect due to their less massive dark matter halos. It shows that the dwarf satellite galaxies around NGC 1291 is somewhat less quenched than those in other system. It is noteworthy that although host galaxies resemble each other in terms of stellar mass, the evolution of dwarf satellite galaxies around them can vary.

4.2. Cumulative luminosity functions

We examined the cumulative luminosity function (LF) of the NGC 1291 system. The Schechter function (Schechter 1976) was employed, which is:

$$N(< M) = \phi^* \Gamma[\alpha + 1, 10^{0.4(M^* - M)}], \quad (3)$$

where $N(< M)$ is the number of galaxies brighter than M , ϕ^* is a scaling factor, α is the faint-end slope, M^* is the characteristic magnitude where the break of LF occurs, and Γ is the upper incomplete gamma function. To improve the completeness of the LF, we included potential members of the NGC 1291 system using the radial velocity range of $839 \pm 150 \text{ km s}^{-1}$ (ESO 300-14; $M_R \simeq -17.79$, ESO 300-16; $M_R \simeq -14.73$). Their projected distances from the center of NGC 1291 are $\simeq 230$ kpc and $\simeq 280$ kpc, respectively. Note that the velocity offset of 150 km s^{-1} for NGC 1291 was defined based on the velocity distribution of nearby objects, but it did not significantly affect the slope of the faint-end.

Figure 9 compares the cumulative LF of the faint galaxies in the NGC 1291 system with those of the MW&M31 (McConnachie 2012; Martin et al. 2013a,b), M83 (Müller et al. 2015), M94 (Karachentsev et al. 2013; Smercina et al. 2018), M101 (Bennet et al. 2019), M106 (Kim

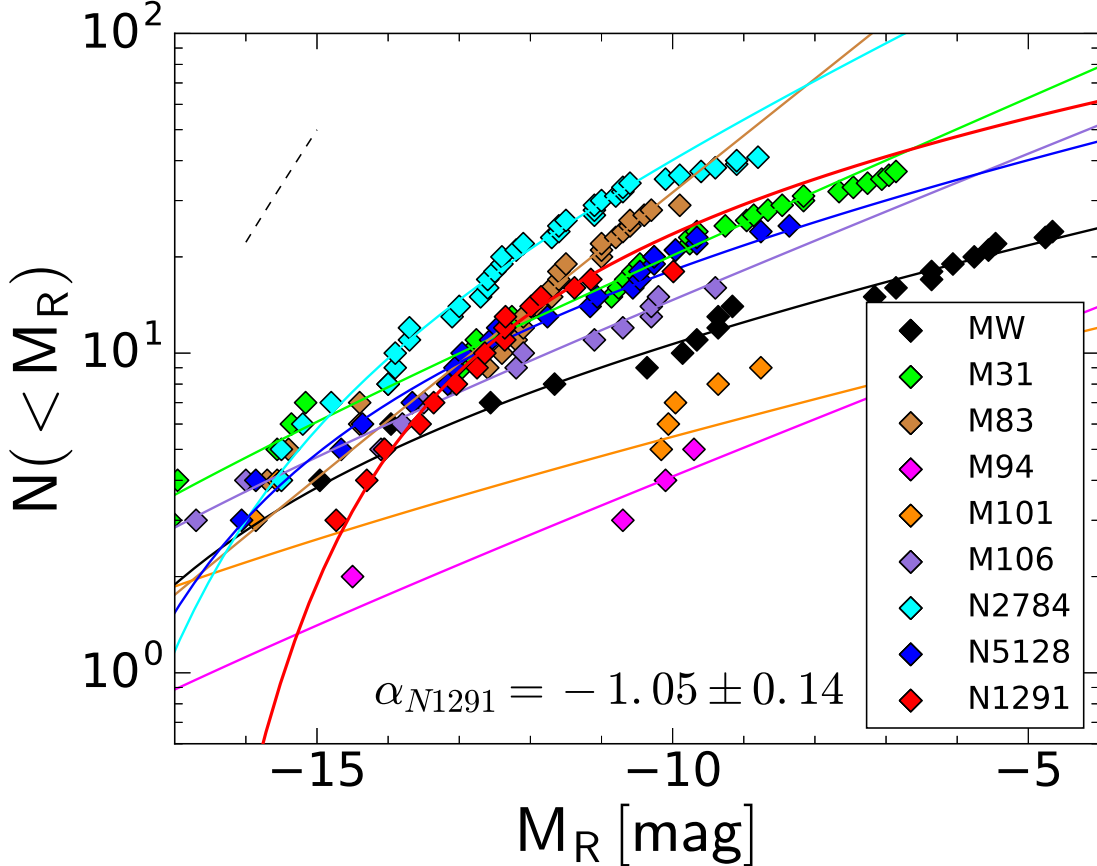


Figure 9. The cumulative luminosity functions of satellite galaxies in the NGC 1291 system and several other host systems. Different colors denote different systems, as labeled in the plot. The solid lines show the fitted Schechter functions using galaxies in $M_R \gtrsim -17$ mag, which also have a completeness rate $>90\%$. The faint-end slope of the NGC 1291 system is noted at the bottom. The dashed line represents the faint-end slope predicted from the Λ CDM model.

et al. 2011), NGC 2784 (Park et al. 2017), NGC 5128 (Crnojević et al. 2019). Note that the incompleteness introduced from the different FoV covered by each study may affect the following results. Since the dwarf satellites in M83, M106, NGC 2784 and NGC 1291 have not yet been confirmed to be located at each host system, the resulting LFs can be regarded as upper limits at the moment. In order to directly compare the references, only galaxies with absolute magnitudes of $M_R^6 \gtrsim -17$ mag were

⁶ For the sake of simplicity, we used the conversion factor of $V - R = 0.56$, $r - R = 0.24$ from Fukugita et al. (1995)

used. The faint magnitude limits of the samples were adopted to have a completeness rate higher than 90% in each study. We found that the faint-end slope in the NGC 1291 system is $\alpha = -1.05 \pm 0.14$, which is much flatter than that predicted by the Λ CDM model ($\alpha = -1.8$; Trentham & Tully 2002) shown as dashed line in Figure 9. It is similar to that of the MW (-1.10 ± 0.07), M31 (-1.24 ± 0.13), M83 (-1.44 ± 0.06), M94 (-1.22), M101 (-1.13), M106 (-1.22 ± 0.17), NGC 2784 (-1.26 ± 0.06), NGC 5128 (-1.11 ± 0.18). Note that we could not derive uncertainties for M94 and M101 because of their sparse satellite populations in the system. This result may indicate that the pop-

ulation of low-mass dwarf galaxies in the NGC 1291 system is indistinct from those in other host systems.

5. SUMMARY

In this study, 15 dwarf galaxy candidates were identified by visual inspection of deep and wide-field images of NGC 1291 obtained with KMT-Net. Of those 15 candidates, 11 are newly discovered in this study. We performed imaging simulations and estimated the completeness of the visual inspection that was above 70% in $\mu_{0,R} \lesssim 26$ mag arcsec⁻² and $M_R \lesssim -10$ mag. The photometric and structural properties of dwarf candidates were measured, the results of which are summarized as follows.

1. The surface brightness profiles of dwarf galaxy candidates were well described with a single Sérsic function. The structural and photometric properties were similar to those of ordinary dwarf galaxies, with a central surface brightness of $\mu_{0,R} \sim 22.5\text{--}26.5$ mag arcsec⁻² and effective radii of 0.2–1 kpc. Assuming that they are located at 9.08 Mpc, the absolute magnitudes of the 15 dwarf galaxy candidates are $-14.5 \lesssim M_R \lesssim -10$ mag.
2. Only the two nearest dwarf candidates from NGC 1291 exhibited nucleated cores. The colors of the dwarf candidates seem to be linearly correlated with their projected distances from the center of NGC 1291. This result may have been a product of the interaction between the host and satellite galaxies, such as tidal interactions and the quenching process.

3. In order to understand the evolution of dwarfs in different environments, the properties of the dwarf candidates were compared to those in other host systems. The color distribution of dwarf candidates is the only property dissimilar from those of other dwarfs in other satellite population systems as the candidates are slightly bluer than other dwarfs. This result indicates that the dwarfs in the NGC 1291 system are likely less quenched than dwarfs in other host systems. It also reveals that environments play an important role in the quenching process but may not affect the morphology shaping of dwarf galaxies.

We are grateful to an anonymous referee for constructive comments and suggestions. This research has made use of the KMTNet system operated by the Korea Astronomy and Space Science Institute (KASI) and the data were obtained at CTIO in Chile, one of three host sites. LCH was supported by the National Science Foundation of China (11721303, 11991052) and the National Key R&D Program of China (2016YFA0400702). This research was supported by the National Research Foundation of Korea (NRF) grant funded by the Korea government (MSIP; NRF-2017R1C1B2002879). YKS acknowledges support from the National Research Foundation of Korea (NRF) grant funded by the Ministry of Science and ICT (NRF-2019R1C1C1010279). H.S.P. was supported in part by the National Research Foundation of Korea (NRF) grant funded by the Korea government (MSIT, Ministry of Science and ICT; NRF-2019R1F1A1058228).

REFERENCES

- Adami, C., Picat, J. P., Savine, C., et al. 2006, *A&A*, 451, 1159
- Bell, E. F., & de Jong, R. S. 2001, *ApJ*, 550, 212

- Bennet, P., Sand, D. J., Crnojević, D., et al. 2019, *ApJ*, 885, 153
- . 2017, *ApJ*, 850, 109
- Bertin, E. 2006, in *Astronomical Society of the Pacific Conference Series*, Vol. 351, *Astronomical Data Analysis Software and Systems XV*, ed. C. Gabriel, C. Arviset, D. Ponz, & S. Enrique, 112
- Bertin, E., Mellier, Y., Radovich, M., et al. 2002, in *Astronomical Society of the Pacific Conference Series*, Vol. 281, *Astronomical Data Analysis Software and Systems XI*, ed. D. A. Bohlender, D. Durand, & T. H. Handley, 228
- Binggeli, B., & Cameron, L. M. 1991, *A&A*, 252, 27
- Binggeli, B., Sandage, A., & Tammann, G. A. 1985, *AJ*, 90, 1681
- Bosma, A., & Freeman, K. C. 1993, *AJ*, 106, 1394
- Bothun, G. D., Impey, C. D., & Malin, D. F. 1991, *ApJ*, 376, 404
- Boylan-Kolchin, M., Bullock, J. S., & Kaplinghat, M. 2011, *MNRAS*, 415, L40
- Bullock, J. S., & Boylan-Kolchin, M. 2017, *ARA&A*, 55, 343
- Byun, W., Sheen, Y.-K., Ho, L. C., et al. 2018, *AJ*, 156, 249
- Capaccioli, M. 1989, in *World of Galaxies (Le Monde des Galaxies)*, ed. J. Corwin, Harold G. & L. Bottinelli, 208–227
- Capaccioli, M., Spavone, M., Grado, A., et al. 2015, *A&A*, 581, A10
- Carlsten, S. G., Greco, J. P., Beaton, R. L., & Greene, J. E. 2019, *arXiv e-prints*, arXiv:1909.07389
- Chiboucas, K., Karachentsev, I. D., & Tully, R. B. 2009, *AJ*, 137, 3009
- Ciotti, L., & Bertin, G. 1999, *A&A*, 352, 447
- Conroy, C. 2013, *ARA&A*, 51, 393
- Conselice, C. J., Gallagher, John S., I., & Wyse, R. F. G. 2002, *AJ*, 123, 2246
- Crnojević, D., Sand, D. J., Bennet, P., et al. 2019, *ApJ*, 872, 80
- Dalcanton, J. J., Spergel, D. N., Gunn, J. E., Schmidt, M., & Schneider, D. P. 1997, *AJ*, 114, 635
- Davies, J. I., Davies, L. J. M., & Keenan, O. C. 2016, *MNRAS*, 456, 1607
- Ferrarese, L., Côté, P., Cuilland re, J.-C., et al. 2012, *ApJS*, 200, 4
- Fliri, J., & Trujillo, I. 2016, *MNRAS*, 456, 1359
- Font, A. S., Benson, A. J., Bower, R. G., et al. 2011, *MNRAS*, 417, 1260
- Fukugita, M., Shimasaku, K., & Ichikawa, T. 1995, *PASP*, 107, 945
- Garrison-Kimmel, S., Wetzel, A., Bullock, J. S., et al. 2017, *MNRAS*, 471, 1709
- Grant, N. I., Kuipers, J. A., & Phillipps, S. 2005, *MNRAS*, 363, 1019
- Greco, J. P., Greene, J. E., Strauss, M. A., et al. 2018, *ApJ*, 857, 104
- Henkel, C., Javanmardi, B., Martínez-Delgado, D., Kroupa, P., & Teuwen, K. 2017, *A&A*, 603, A18
- Ibata, R. A., Lewis, G. F., Conn, A. R., et al. 2013, *Nature*, 493, 62
- Impey, C., Bothun, G., & Malin, D. 1988, *ApJ*, 330, 634
- Into, T., & Portinari, L. 2013, *MNRAS*, 430, 2715
- Javanmardi, B., Martínez-Delgado, D., Kroupa, P., et al. 2016, *A&A*, 588, A89
- Jerjen, H., Binggeli, B., & Freeman, K. C. 2000, *AJ*, 119, 593
- Karachentsev, I. D., Makarov, D. I., & Kaisina, E. I. 2013, *AJ*, 145, 101
- Kim, E., Kim, M., Hwang, N., et al. 2011, *MNRAS*, 412, 1881
- Kim, S.-L., Cha, S.-M., Lee, C.-U., et al. 2016a, *Publication of Korean Astronomical Society*, 31, 35
- Kim, S.-L., Lee, C.-U., Park, B.-G., et al. 2016b, *Journal of Korean Astronomical Society*, 49, 37
- Klypin, A., Kravtsov, A. V., Valenzuela, O., & Prada, F. 1999, *ApJ*, 522, 82
- Kondapally, R., Russell, G. A., Conselice, C. J., & Penny, S. J. 2018, *MNRAS*, 481, 1759
- Kravtsov, A. V. 2013, *ApJL*, 764, L31
- Kravtsov, A. V., Gnedin, O. Y., & Klypin, A. A. 2004, *ApJ*, 609, 482
- Leisman, L., Haynes, M. P., Janowiecki, S., et al. 2017, *ApJ*, 842, 133
- Li, J.-T., Wang, Q. D., Li, Z., & Chen, Y. 2011, *ApJ*, 737, 41
- Lieder, S., Lisker, T., Hilker, M., Misgeld, I., & Durrell, P. 2012, *A&A*, 538, A69
- Lisker, T., Grebel, E. K., & Binggeli, B. 2006, *AJ*, 132, 497
- Lupton, R. H. 2005, *Transformations between SDSS magnitudes and other systems*, [https://www.sdss.org/dr15/algorithms/sdssubvritransform/#Lupton\(2005\)](https://www.sdss.org/dr15/algorithms/sdssubvritransform/#Lupton(2005))

- Martin, N. F., Slater, C. T., Schlafly, E. F., et al. 2013a, *ApJ*, 772, 15
- Martin, N. F., Schlafly, E. F., Slater, C. T., et al. 2013b, *ApJL*, 779, L10
- McConnachie, A. W. 2012, *AJ*, 144, 4
- McQuinn, K. B. W., Skillman, E. D., Dolphin, A. E., Berg, D., & Kennicutt, R. 2017, *AJ*, 154, 51
- Merritt, A., van Dokkum, P., & Abraham, R. 2014, *ApJL*, 787, L37
- Merritt, A., van Dokkum, P., Danieli, S., et al. 2016, *ApJ*, 833, 168
- Metz, M., Kroupa, P., & Jerjen, H. 2007, *MNRAS*, 374, 1125
- Mihos, J. C., Durrell, P. R., Ferrarese, L., et al. 2015, *ApJL*, 809, L21
- Moore, B., Ghigna, S., Governato, F., et al. 1999, *ApJL*, 524, L19
- Morshidi-Esslinger, Z., Davies, J. I., & Smith, R. M. 1999, *MNRAS*, 304, 297
- Muñoz, R. P., Eigenthaler, P., Puzia, T. H., et al. 2015, *ApJL*, 813, L15
- Müller, O., Jerjen, H., & Binggeli, B. 2015, *A&A*, 583, A79
- Müller, O., Scalera, R., Binggeli, B., & Jerjen, H. 2017, *A&A*, 602, A119
- Oh, K. S., & Lin, D. N. C. 2000, *ApJ*, 543, 620
- Park, H. S., Moon, D.-S., Zaritsky, D., et al. 2019, *ApJ*, 885, 88
- . 2017, *ApJ*, 848, 19
- Paturel, G., Petit, C., Prugniel, P., et al. 2003, *A&A*, 412, 45
- Pawłowski, M. S., Pflamm-Altenburg, J., & Kroupa, P. 2012, *MNRAS*, 423, 1109
- Phillips, J. I., Wheeler, C., Cooper, M. C., et al. 2015, *MNRAS*, 447, 698
- Prole, D. J., Davies, J. I., Keenan, O. C., & Davies, L. J. M. 2018, *MNRAS*, 478, 667
- Sandage, A., & Binggeli, B. 1984, *AJ*, 89, 919
- Schechter, P. 1976, *ApJ*, 203, 297
- Schombert, J. M., Pildis, R. A., Eder, J. A., & Oemler, Augustus, J. 1995, *AJ*, 110, 2067
- Smercina, A., Bell, E. F., Price, P. A., et al. 2018, *ApJ*, 863, 152
- Trentham, N., & Tully, R. B. 2002, *MNRAS*, 335, 712
- Tully, R. B., Libeskind, N. I., Karachentsev, I. D., et al. 2015, *ApJL*, 802, L25
- van der Burg, R. F. J., Muzzin, A., & Hoekstra, H. 2016, *A&A*, 590, A20
- van Dokkum, P. G., Abraham, R., Merritt, A., et al. 2015, *ApJL*, 798, L45
- Venhola, A., Peletier, R., Laurikainen, E., et al. 2017, *A&A*, 608, A142
- . 2019, *A&A*, 625, A143
- Yagi, M., Koda, J., Komiyama, Y., & Yamanoi, H. 2016, *ApJS*, 225, 11
- York, D. G., Adelman, J., Anderson, John E., J., et al. 2000, *AJ*, 120, 1579
- Zaritsky, D., Donnerstein, R., Dey, A., et al. 2019, *ApJS*, 240, 1